ZEOLITE-X ENCAPSULATED Ni(II) AND Co(II) COMPLEXES WITH 2,6-PYRIDINE DICARBOXYLIC ACID AS CATALYSTS FOR OXIDATIVE DEGRADATION OF ATENOLOL IN AN AQUEOUS SOLUTION

Fatemeh Hassani[1], Mahboubeh A. Sharif[2*], Masoumeh Tabatabaee[1] and Mahboobeh Mahmoodi[3]

[1]Department of Chemistry, Yazd Branch, Islamic Azad University, Yazd, Iran
[2]Production and Recycling of Materials and Energy Research Center, Qom Branch, Islamic Azad University, Qom, Iran
[3]Department of Biomedical Engineering, Yazd Branch, Islamic Azad University, Yazd, Iran

ABSTRACT. Complexes of Co(II) and Ni(II) with 2,6-pyridine dicarboxylic acid ($PydcH_2$) have been synthesized in the NaX (zeolite-X) nanopores. The formation of zeolite X encapsulated Co(II) and Ni(II) complexes ($[M(pydcH)_2]$-NaX, $[M = Co(II)$ and $Ni(II)]$) were confirmed using spectroscopic methods of FT-IR, elemental analysis, XRD, FE-SEM, and TEM. It was affirmed that the encapsulation of complexes in NaX pores was formed without changes in the structure and shape of the zeolite. The oxidative degradation reaction of atenolol with hydrogen peroxide as an oxidant was performed in the presence of synthesized $[M(pydcH)_2]$-NaX nanocomposites to study their catalytic activity. Therefore, oxidation of atenolol was performed under different conditions of catalyst, temperature, and time. Under optimal conditions, catalysts $[Co(pydcH)_2]$-NaX and $[Ni(pydcH)_2]$-NaX showed 82.3% and 71.1% activity of atenolol oxidation, respectively. These catalysts were stable after recovery and were used three more times. The results showed that these catalysts were reusable and had a reduction in the catalytic activity of less than ten percent.

KEY WORDS: Zeolite-X, Nano porosity, Ion-exchange, Degradation of atenolol, 2,6-Pyridine dicarboxylic acid

INTRODUCTION

Today, the pharmaceutical and health industries have caused the entry of various pollutants into the environment and water resources, and as a result, threaten the health of the people. Therefore, removing them from the environment becomes more important [1-4]. Typically, drugs either absorb activated sludge and enter the sludge digesters and can play a role in inhibiting the biodegradation activity of anaerobic bacteria, or by entering conventional wastewater treatment processes with effluent, entering soil or surface water, groundwater and then drinking water [5-7].
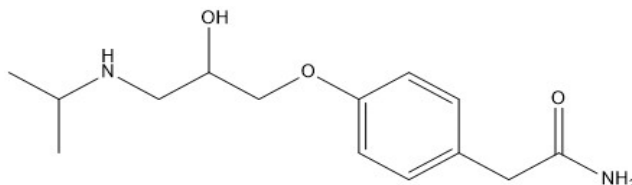
Scheme 1. Structure of the atenolol.

Medicinal compounds, including cardiovascular drugs, are substances that are very useful and despite their side effects, they are widely used in medicine [8-11]. Among these drugs is one of

*Corresponding author. E-mail: m_sharif@qom-iau.ac.ir ; mahboubeh.sharif@yahoo.com

the most widely used cardiovascular drugs called atenolol (Scheme 1), which is one of the most widely used drugs due to the prevalence of cardiovascular disease and hypertension. Atenolol is a beta-blocker and is used to treat chronic angina, high blood pressure (alone or with other antihypertensive drugs) and to prevent myocardial infarction [12]. About 50 to 60% of the drug is absorbed from the gastrointestinal tract. Many drugs are low protein-bonded in plasma, so they are metabolized in small amounts in the liver, the biological half-life of the drug is 6-7 h. and the time required to reach the peak effect is 2-4 h, 85 to 100% of the drug is unchanged by the kidney.

Pharmaceutic compounds mainly have high endurance and low biodegradability. These pharmacokinetic factors are considered beneficial parameters to extend the half-life of the drug in the human body. Accordingly, these pharmaceutical residues also contribute to their increased persistence in the environment. However, the continuous release in large quantities, and a slower rate of auto-degradation of these pharmaceutical residues, build up the contamination from ng/L to μg/L. This poses adverse impacts on human health, life under water, and facilitates the development of antimicrobial resistant microbes [13-15]. Therefore, it is necessary to provide a simple, sensitive, and fast method to remove drugs from aqueous sources [16-18]. Many methods are used to remove these compounds, including membrane processes such as nanofiltration, ultrafiltration, reverse osmosis, etc., that their disadvantages are high pressure, high cost of the membrane, and most importantly chemical or microbial clogging of the membrane that prevents water from passing through the filter and reducing the flow [19]. Conventional oxidation treatment is another method of removing contaminants by adding an oxidizing agent to a solution containing contaminants. With this oxidation, some of the contaminants are removed and decomposed. In wastewater treatment, oxidizers such as chlorine and other chlorine-containing compounds (such as hypochlorous acid), oxygen, ozone, and hydrogen peroxide are used for oxidation. Chlorine and its derivatives can be used in the role of chemical oxidant in wastewater treatment. However, due to its high oxidation strength, it reacts with aromatic rings and double bond substances, which result in halogenated organic matter, and some of them have the potential for carcinogenic risk. Therefore, the use of chlorine in the decomposition of wastewater organic matter is not appropriate [20, 21]. So, catalytic oxidation with H_2O_2 in the presence of an appropriate catalyst is considered.

Transition metal complexes of transfer elements are good catalysts and some of them have high solubility in solution, so they are considered homogeneous catalysts [22, 23]. Although homogeneous catalysts have high activity and selectivity, but the difficulty of separating them from the product limits their industrial applications. This problem can be solved by heterogeneizing them [24-26]. Homogeneous catalysts can be converted to heterogeneous catalysts by bonding or encapsulation [27, 28].

Zeolites are crystalline aluminosilicates with cavities and channels of the specified size and unique properties such as ion exchange, adsorption, and catalytic activity which are very suitable in industrial applications. [29]. The general oxide formula for NaX zeolite is $Na_2O.Al_2O_3.5SiO_2$ and for its unit cell is ($Na_{88}Al_{88}Si_{104}O_{384}.172.1H_2O$). The NaX zeolite is of the Fujasite family and the sodalite cages are connected by the secondary prismatic units with a hexagonal base. The size of the cavity and its channels is about 0.74 nm (relatively large), and it is used as a stable size in the production of catalysts [30].

To increase the catalytic activity of the complexes, they can be encapsulated in the pores and cavities of the inorganic polymer structure [31-35]. Zeolites are unique among all types of compounds with porous and porous structures, because they have a regular crystal structure with high chemical and thermal stability. The proper structure of zeolites has made them a suitable environment for trapping active metal complexes and metal clusters, which use these modified systems as catalysts [36]. There are three methods for encapsulating coordination compounds in the pores and channels of zeolite, including the method and synthesis of zeolite complexation, the template synthesis method and the synthesis method, and the flexible ligand method, simultaneously [37, 38].

In this research work, the flexible ligand method has been used. First, the appropriate metal enters the zeolite structure by ion exchange method, and then the appropriate ligand in terms of size and flexibility is spread in the zeolite structure, in this method. The ligand used in this method must have sufficient flexibility to be stable and not be degraded during adsorption and binding to the exchanged metal in the zeolite pores. The amount of complex produced in the zeolite pores is proportional to the amount of cation exchanged with the sodium cations in the zeolite structure. The excess amount of ligand and metal complex on the outer surface of the zeolite should be separated by a solvent.

Continuing the previous work [39], we describe the synthesis and characterization of the encapsulated Ni(II) and Co(II) complexes of $pydcH_2$ in zeolite-X and their use in the oxidation of atenolol (an organic pollutant in wastewater) with hydrogen peroxide as an oxidant.

EXPERIMENTAL

Materials and Physical methods of analysis

All materials required for the synthesis of compounds were purchased commercially from Sigma Aldrich or Merck. The FT-IR spectra of the synthesized solids were recorded with KBr tablets in the range of 4000-400 cm^{-1} by a Bruker Tensor 27 FT-IR-spectrophotometer. The TESCAN, Mira 3-XMU field-emission scanning electron microscope (FE-SEM) and transmission electron microscopy (TEM) (Zeiss-EM10C-80KV) were used to examine the morphology of the samples and particle shape, respectively. To study the structure and phase detection in the synthesized samples, X-ray diffraction (XRD) was used and it was applied to the surface of the sample by CuKα on a Philips, X'Pert PRO. Perkin-Elmer Optima 2000 DV ICP-AES was used for elemental analysis of samples. The UV-Vis spectra were recorded at 254 nm using the Avantes spectrophotometer (AvaSpec-ULS2048LTEC).

Preparation of zeolite-X

Synthesized zeolite-X was used as a substrate in the laboratory [40]. Sodium silicate and sodium aluminate were used as raw materials in the preparation of zeolite X. To prepare sodium silicate, a mixture of silica gel (3 g), sodium hydroxide (2.4 g, 0.06 mol), and deionized water (6 mL) was stirred to give a clear solution. Sodium aluminate solution was obtained by mixing aluminum isopropoxide (6.9 g, 0.03 mol), sodium hydroxide (2.4 g, 0.06 mol), and deionized water (9 mL) in another beaker. Stirring was continued for about ten minutes (below 80 °C) until the material was completely dissolved and a clear solution was obtained. Evaporation of water was prevented by placing the watch glass on the beaker. After both solutions reached room temperature, the aluminum silicate solution was added to the sodium silicate solution. Then 27 mL of water was added and the reaction mixture was stirred to form a perfectly homogeneous mixture. The mixture was immediately transferred to a polypropylene container with a screw cap and placed in an oven at 90 °C for 3-4 h. The reaction mixture was then cooled to room temperature. After sediment settling, the mixture was filtered and washed with plenty of deionized water until the *p*H of the washing liquid became neutral, but no smoothing method was used to wash away the residue. Finally, the white zeolite X crystals were dried in an oven or at room temperature.

Preparation of [M(pydcH₂)₂)]-NaX (M = Ni and Co)

Zeolite X was used to synthesize nanocomposite catalysts through encapsulating nickel(II) and cobalt(II) complexes in zeolite pores. In this regard, the flexible ligand method was used in the following two steps.

The exchanged M(II) zeolite-X (M (II)-NaX) was prepared according to the method described in the literature [41]. Zeolite X (4 g) was transferred to a 250 ml in reaction flask together with deionized water (250 ml) and 4 mmol $M(NO_3)_2$. The suspension was refluxed for 24 h. at 90 °C. Then, the mixture was filtered and the precipitate was washed several times with deionized hot water. The precipitate was placed in an oven for 15 h at 150 ° C to dry completely.

The dry precipitate (1 g) obtained from the before step was placed in a 250 mL balloon and placed in an oil bath. 12 mmol of pyridine 2,6 dicarboxylic acid ligand and 100 mL of ethanol were added to the precipitate and refluxed for 24 h at 90 °C. Then the mixture was placed in a smooth oven at 150 °C to dry completely. To remove unreacted ligands, the precipitate was soaked with ethanol and acetonitrile for 6 h, respectively. After drying, the resulting mixture was placed in a solution of sodium chloride (100 ml, 0.01 M) for 24 h (for the removal of uncoordinated metal ions from the zeolite cavities). After filtering the reaction mixture and washing the precipitate with deionized water several times, it was dried at 120 °C.

Catalytic reaction for the oxidation of atenolol

An aqueous solution of atenolol (10 mL, 2 ppm), was prepared and its absorption was measured at 254 nm by spectrophotometer. Then different amounts of catalyst (0.005, 0.01, and 0.015 g) and hydrogen peroxide (0.01, 0.02, 0.03 and 0.04 ml, 30 wt.%, as an oxidant) were added to the solution and were stirred at ambient temperature (30 °C) for 30, 60 and 180 min. The mixture was centrifuged and the absorption of clear solution was measured in the range of 250-700 nm. To recover the catalyst, the residue was filtrated and washed with solvents for reuse.

RESULTS AND DISCUSSION

Both the Co(II) and Ni(II) ions coordinated with $pydcH^-$ were encapsulated in the pores of zeolite X by the Flexible Ligand Method [41]. First, Na^+ ion was exchanged with M(II) ion and then the complex formation was performed in M(II) -X zeolite cavities by adding an additional amount of the $pydcH_2$ (Scheme 2). The $pydcH_2$ can diffuse simply *via* the zeolite pores because of its flexible nature and then the complexes of $[M(pydcH)_2]$ were formed in the zeolite pores [42]. So, the prepared complex inside the cages of zeolite is too large to come out of the pores. To remove excess of the ligand inside the pores as well as located on the surface of zeolite the precipitate was Soxhleted in ethanol and acetonitrile for 6 h, respectively.
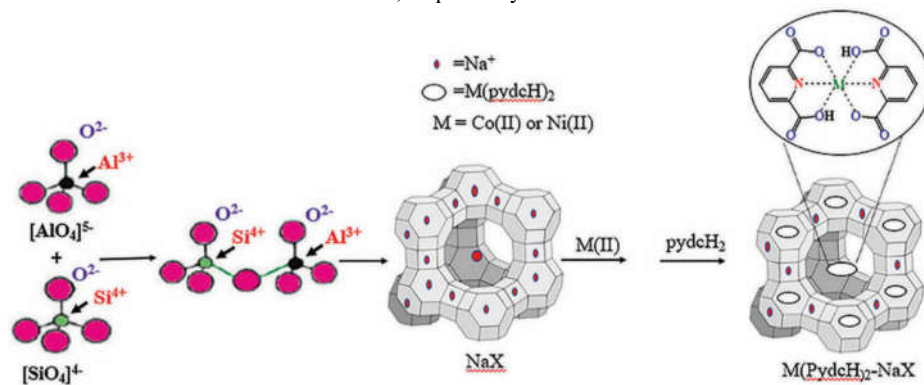
Scheme 2. Encapsulation of Ni(II) and Co(II) complexes with 2,6-pyridine dicarboxylic acid in zeolite-X.

Characterization of [M(pydcH)₂)]-NaX

FT-IR spectroscopy

The FT-IR spectra of NaX and encapsulated Co(II) and Ni(II) complexes (catalysts) are shown in Figure 1. The study of FT-IR spectra of different zeolites shows the presence of two groups of vibrating bands in these compounds. The first group is bands that are related to the internal vibrations of the tetrahedral TO_4 (T = Al, Si). These bands are not sensitive to the overall structure of the zeolite and are often seen in all zeolite structures. The second group of bands is found only in some zeolite structures and is therefore attributed to the connections between the tetrahedral anions. The intensity of this group of bands is reduced or disappeared completely if the zeolite structure is destructed [43]. The bands around 3450 cm^{-1} (broad) and 1642 cm^{-1} have related to the stretching and bending modes of water molecules adsorbed by the zeolite X, respectively [40]. The band appearing at 1010 cm^{-1} is also attributed to the quadrilateral Si-O-Al tensile vibration. Symmetric T-O-T stretching, six-membered rings of T-O-T symmetric stretching, and Si-O-Si symmetric stretching are assigned by absorption bands at 764, 582, and 657 cm^{-1}, respectively. Also, the symmetric bending of the modes of T-O is assigned by the band at 480 cm^{-1}. These findings are similar to previous studies and this proves the formation of zeolite X in this work [44, 45].
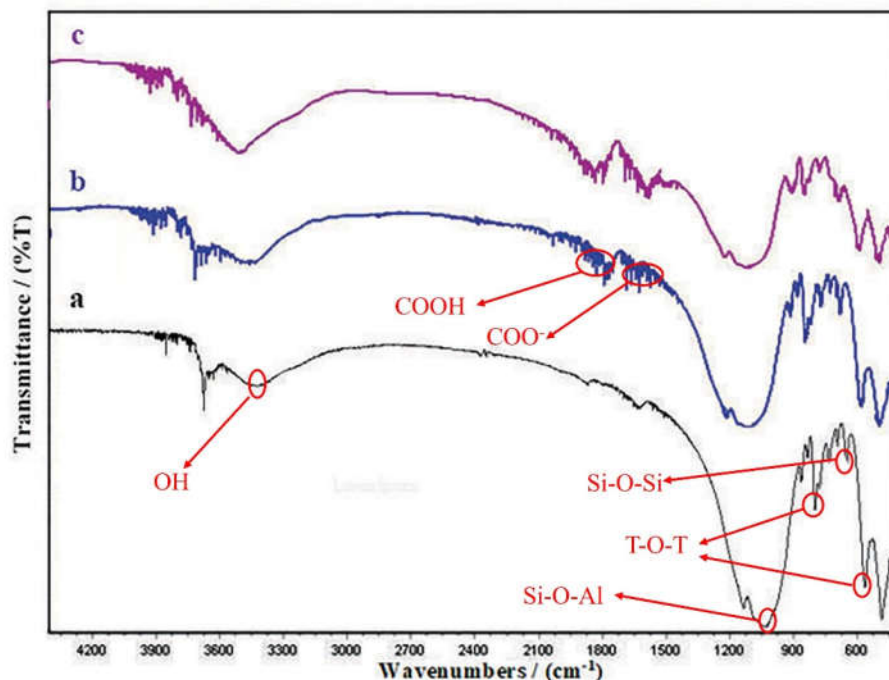
Figure 1. FTIR spectra of (a) NaX, (b) [Co(pydcH)₂]-NaX and (c) [Ni(pydcH)₂]-NaX.

IR spectroscopy also provides good information about encapsulated metal complexes and the crystal structure of the host zeolite. In the spectrum of both samples, the absorption bands are affected by the crystal structure of the zeolite [46]. In the range of 3700-3300 cm^{-1}, vibrations

related to hydroxyl groups can be detected (corresponding to the connections of the OH group of ligands). The fact that the main vibrations in the structure of the zeolite have not changed or significantly expanded can be confirmed that the process of encapsulation of the complexes has not changed the framework of the zeolite. The relevant bands are weakened in composites, due to the low concentration of complexes, and therefore it is observed only in areas such as 1830 and 1790 cm^{-1} resulting from stretching vibrations of carbonyl (C=O) or carboxyl (COOH) groups for $[Co(pydcH)_2]$-NaX and $[Ni(pydcH)_2]$-NaX, respectively. The bands assigned to the asymmetric stretches ($\nu_{as}COO^-$) were in the range 1680–1635 cm^{-1} (for $[Co(pydcH)_2]$-NaX) and 1645–1575 cm^{-1} (for $[Ni(pydcH)_2]$-NaX), whereas a somewhat weaker symmetric stretches ($\nu_{sym}COO^-$) at 1580 and 1510 cm^{-1} for nickel(II) and cobalt(II) complexes encapsulated in zeolite, respectively [47]. Various coordinating modes exists in the 2,6-pyridinedicarboxylic acid complexes which can be distinguished from the difference in asymmetric and symmetric carboxylate stretching bands, $\Delta \nu = \nu_{as}COO^- - \nu_{sym}COO^-$. If there is a marked difference of over 200 cm^{-1} it implies monodentate coordination while a difference of about 100 cm^{-1} confirms a bidentate coordination. The small difference between ν_{as} and ν_{sym} ($\Delta \nu < 200$ cm^{-1}) frequencies indicates bidentate coordination [47].

Analytical data

The ICP-AES analytical data of NaX, M(II)-NaX, and ($[M(pydcH)_2]$-NaX nanocomposites are shown in Table 1. The Si/Al molar ratio in NaX is 1.22 which is in agreement with the unit cell formula ($Na_{88}Al_{88}Si_{104}O_{384}$) [48]. The Si/Al ratio remained unchanged in M(II)-NaX, indicating no occurrence of dealumination during the ion exchange. The M/N molar ratio in M-pydc-NaX shows only a slight distortion comparison with the free complex), which confirmed that the structure of the complex in the zeolite channels did not change. The contents of M, C, H, and N metal to ligand ratio of about 1:2 for $[M(pydcH)_2]$-NaX. However, slightly lower molar ratios in each case show a small trace of free metal ions in the lattice.

According to the Si/Al ratio in M(II)-NaX remains unchanged indicating the absence of dealumination during ion exchange. It also confirms that the structure of zeolite channels has not changed after ion exchange and complex formation in cavities. The values of M, C, H, N indicate the metal to ligand ratio of about 1:2 for $[M(pydcH)_2]$-NaX.

Table 1 ICP-AES analytical data for NaX, M(II)-NaX and $[M(pydcH)_2]$-NaX; M = Co, Ni.

Compound	%M	%C	%N	%Si	%Al	%Na	M/N	Si/Al
NaX	-	-	-	20.56	16.84	16.92	-	1.22
Co-NaX	5.20	-	-	20.36	16.72	12.25	-	1.22
$[Co(pydcH)_2]$-NaX	3.84	10.58	1.78	20.13	16.47	14.01	0.51	1.22
Ni-NaX	4.32	-	-	20.72	16.93	13.53	-	1.22
$[Ni(pydcH)_2]$-NaX	3.23	8.74	1.46	19.33	15.81	14.87	0.52	1.22

Powder X-ray diffraction

The XRD pattern of NaX, M(II) exchanged zeolite-X, and ($[M(pydcH)_2]$-NaX) were obtained at $2\theta = 0°$ - $70°$ are shown in Figure 2. The crystal phases of the synthesized material can be determined by comparing the X-ray diffraction pattern and the ASTM cards. As shown in the figure, the XRD pattern of the Zeolite X is the same as the standard zeolite-X [41]. The absence of additional peaks in the XRD pattern indicates the synthesis of high purity zeolite-X. According to Figure 2, a little displacement in the peaks of the complexes indicate that the process of catalyst synthesis (ion exchange and encapsulation of the complexes) based on zeolite has caused minor changes in the distance of its crystal planes, but in general, the structure and zeolite framework of

NaX remain stable during the preparation process of composites. The average nano crystallite sizes (measured from the X-ray diffraction line broadening pattern) are 34.12, 40.17, 24.68, 42.62 and 20.50 nm for NaX, Co-X, Ni-X, [Co(pydcH)$_2$]-NaX and [Ni(pydcH)$_2$]-NaX, respectively.
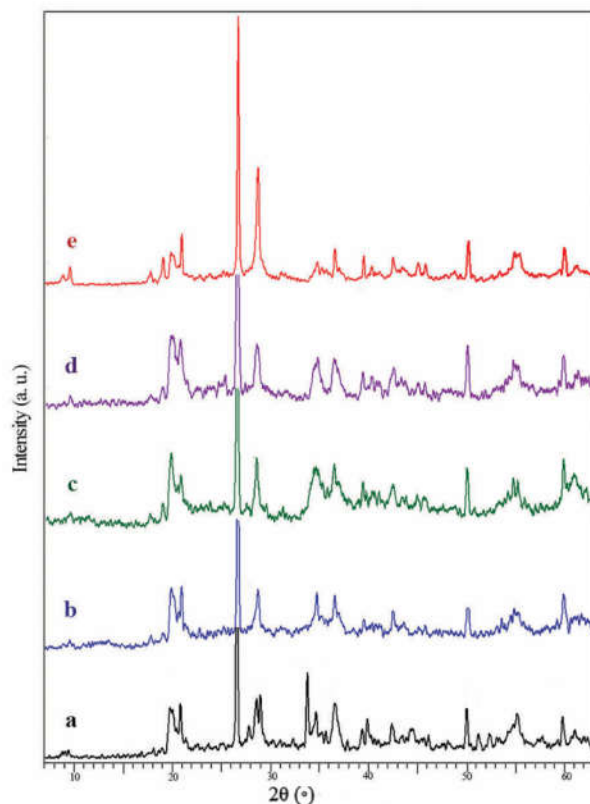
Figure 2. XRD patterns of (a) NaX, (b) Co-X, (c) Ni-X, (d) [Co(pydcH)$_2$]-NaX and (e) [Ni(pydcH)$_2$]-NaX.

Scanning/transmission electron microscopy

Scanning electron microscopy (SEM) Images of NaX and [M(pydcH)$_2$)]-NaX is shown in Figure 3. The sample particles have an irregularly shaped angle, an almost smooth surface, and multilayer sheets. These images show that the exchanged ions and complexation are mostly inside the pores of the zeolite X.

TEM images of [M(pydcH)$_2$]-NaX are shown in Figure 4. These pictures show that the structure of all of them is rectangular cubic. The [Ni(pydcH)$_2$]-NaX and [Co(pydcH)$_2$]-NaX also show slightly opaque and regular form but a little change at the surface margin. In addition, partial aggregation is considered compared to the parent zeolite. Due to the encapsulation of complex sections in zeolite channels, the morphology of [Ni(pydcH)$_2$]-NaX and [Co(pydcH)$_2$]-NaX show a crystalline nature. TEM images show an average length of 31.58±9 nm and 44.41±17 nm for [Ni(pydcH)$_2$]-NaX and [Co(pydcH)$_2$]-NaX, respectively. Images of [Ni(pydcH)$_2$]-NaX and [Co(pydcH)$_2$]-NaX show the absence of M (II) complex traces on the surface.
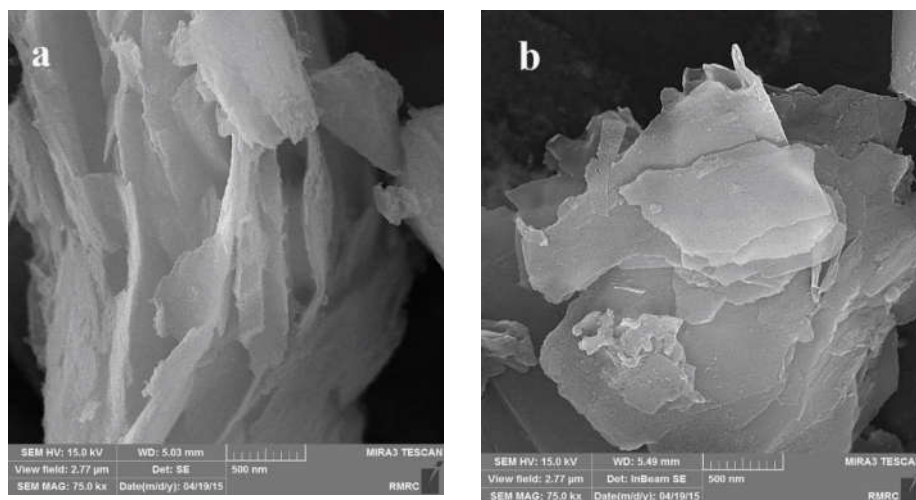
Figure 3. SEM images of the (a) [Co(pydcH)$_2$]-NaX and (b) [Ni(pydcH)$_2$]-NaX.
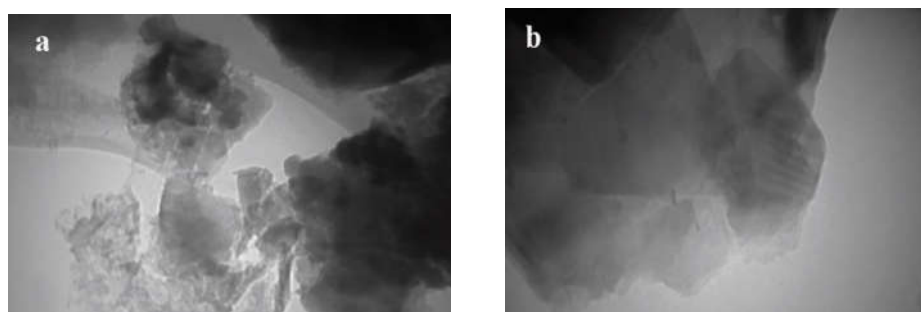
Figure 4. TEM images of the (a) [Co(pydcH)$_2$]-NaX and (b) [Ni(pydcH)$_2$]-NaX.

Catalytic activity (oxidation of atenolol)

The catalytic activity of [Ni(pydcH)$_2$]-NaX and [Co(pydcH)$_2$]-NaX composites in the degradation oxidation reaction of a solution of atenolol (10 mL, 20 ppm) in the presence of H$_2$O$_2$ were investigated. Process optimization was performed by the change of different parameters such as reaction time (30, 60, 90, 120, and 180 min), the amount of catalyst (5, 10, 15, 20, 25 mg), and the volume of hydrogen peroxide (0.01, 0.02, 0.03 and 0.04 mL) at 30 °C under conditions where all other factors were constant (Table 2).

The concentration of residual atenolol was calculated using a spectrophotometer at 254 nm according to the following equation:

$$R = \frac{(C_0 - C_1)}{C_0} * 100$$

where C$_0$ and C$_t$ indicate the initial and final concentration of the atenolol (after the degradation process), respectively.

The results showed that the oxidative degradation of atenolol increased with enhancement time. Since there was a slight increase in efficiency after 60 min, the optimize time was considered 60 min.

To find the optimal amount of catalyst, atenolol degradation was performed in different amounts of catalyst from 5 to 25 mg. Oxidation efficiency of 71.1 % and 82.3 % was obtained after 60 min of reaction at 30 °C with 10 mg of catalyst in the presence of [Ni(pydcH)$_2$]-NaX and [Co(pydcH)$_2$]-NaX, respectively (Table 2). The degradation of atenolol becomes greater with increasing the amount of catalyst up to 15 mg, but an additional increase in the amount of catalyst reduces the oxidation performance of atenolol due to lower access to active sites. In addition, excess catalyst leads to the decomposition of H$_2$O$_2$, which ultimately prevents the oxidative degradation reaction [49].

Homogeneous complex compounds are not recyclable as a catalyst even once and lose their catalytic activity after use. However, heterogeneous catalysts can be reused after catalytic filtration and washing without major damage to catalytic activity [50]. After completion of the reaction, filtration and separation of the catalyst, and then washing with a solvent, the catalyst was reused under similar conditions. The atomic absorption spectroscopy of catalysts did not show any loss of nickel or cobalt after reuse, although their catalytic activity was slightly reduced.

Table 2. Effect of various parameters on the catalytic oxidative degradation of atenolol.

Catalyst	Time (min)	Catalyst (mg)	H$_2$O$_2$ (mL)	Degradation (%)
[Co(pydcH)$_2$]-NaX	30	5	0.01	28.2
	60	5	0.01	55.1
	90	5	0.01	59.2
	120	5	0.01	59.8
	180	5	0.01	60.1
	60	5	0.01	55.1
	60	10	0.01	75.6
	60	15	0.01	75.9
	60	20	0.01	74.3
	60	25	0.01	71.2
	60	10	0.01	75.6
	60	10	0.02	79.8
	60	10	0.03	81.2
	60	10	0.04	82.3
[Ni(pydcH)$_2$]-NaX	30	5	0.01	23.6
	60	5	0.01	48.3
	90	5	0.01	51.7
	120	5	0.01	52.3
	180	5	0.01	52.8
	60	5	0.01	48.3
	60	10	0.01	59.8
	60	15	0.01	60.1
	60	20	0.01	57.9
	60	25	0.01	53.6
	60	10	0.01	59.8
	60	10	0.02	67.3
	60	10	0.03	70.4
	60	10	0.04	71.1

CONCLUSION

The aim of this study was to remove atenolol from aqueous solutions using the oxidative degradation reaction in the presence of [Co(pydcH)$_2$]-NaX and [Ni(pydcH)$_2$]-NaX

nanocomposites as a catalyst. The results showed that the catalysts were synthesized correctly and the cobalt complex with pyridine-2,6-dicarboxylic acid was encapsulated to a greater extent than the nickel complex in the zeolite X cavities. According to the molar ratio of metal to nitrogen, it can be concluded that the molar ratio of metal to the ligand is 1:2. The catalytic degradation of atenolol shows that [Co(pydcH)$_2$]-NaX nanocomposite has more activity than [Ni(pydcH)$_2$]-NaX, due to the amount of complex encapsulation in the zeolite X cavities. Degradation of atenolol increases with enhancement temperature, time, and amount of hydrogen peroxide in the presence of both complexes. Although the oxidation percentage of atenolol increases in the presence of catalyst up to 10 mg, but the percentage of oxidation of atenolol decreases by the excess amount of catalyst because of the decomposition of H$_2$O$_2$. In addition, the removal efficiency of atenolol showed a reduction of less than 10% in the reuse of catalysts for three periods.

ACKNOWLEDGMENTS

REFERENCES

1. Bolong, N.; Ismail, A.F.; Salim, M.R.; Matsuura, T. A review of the effects of emerging contaminants in wastewater and options for their removal. *Desalination* **2009**, 239, 229-246.
2. Quesada, H.B.; Baptista, A.T.A.; Cusioli, L.F.; Seibert, D.; Bezerra, C.O.; Bergamasco, R. Surface water pollution by pharmaceuticals and an alternative of removal by low-cost adsorbents: A review. *Chemosphere* **2019**, 222, 766-780.
3. Tijani, J.O.; Fatoba, O.O.; Petrik, L.F. A review of pharmaceuticals and endocrine-disrupting compounds: sources, effects, removal, and detections. *Water Air Soil Pollut.* **2013**, 224, 1770.
4. Teodosiu, C.; Gilca, A.F.; Barjoveanu, G.; Fiore, S. Emerging pollutants removal through advanced drinking water treatment: A review on processes and environmental performances assessment. *J. Clean. Prod.* **2018**, 197, 1210-1221.
5. Liao, Q.; Rong, H.; Zhao, M.; Luo, H.; Chu, Z.; Wang, R. Interaction between tetracycline and microorganisms during wastewater treatment: A review. S*ci. Total Environ.* **2021**, 757, 143981.
6. Luo, J.; Zhang, Q.; Zhao, J.; Wu, Y.; Wu, L.; Lia, H.; Tang, M.; Sun, Y.; Guo, W.; Feng, Q.; Cao, J.; Wang, D. Potential influences of exogenous pollutants occurred in waste activated sludge on anaerobic digestion: A review. *J. Hazard. Mater.* **2020**, 383, 121176.
7. Huang, X.; Xu, Q.; Wu, Y.; Wang, D.; Yang, Q.; Chen, F.; Wu, Y.; Pi, Z.; Chen, Z.; Li, X.; Zhong, Q. Effect of clarithromycin on the production of volatile fatty acids from waste activated sludge anaerobic fermentation. *Bioresour. Technol.* **2019**, 298, 121598.
8. Proschak, E.; Stark, H.; Merk, D. Polypharmacology by design: a medicinal chemist's perspective on multitargeting compounds. *J. Med. Chem.* **2019**, 62, 420-444.
9. Anand, U.; Jacobo-Herrera, N.; Altemimi, A.; Lakhssassi, N. A comprehensive review on medicinal plants as antimicrobial therapeutics: potential avenues of biocompatible drug discovery. *Metabolites* **2019**, 9, 258.
10. Tungmunnithum, D.; Thongboonyou, A.; Pholboon, A.; Yangsabai, A. Flavonoids and other phenolic compounds from medicinal plants for pharmaceutical and medical aspects: An overview. *Medicines* **2018**, 5, 93.
11. Rastogi, S.; Pandey, M.M.; Rawat, A.K.S. Traditional herbs: a remedy for cardiovascular disorders. *Phytomedicine* **2016**, 23, 1082-1089.
12. Ong, H.T. Beta blockers in hypertension and cardiovascular disease. *B. M. J.* **2007**, 334, 946-949.

13. Jobin, G.; Cortot, A.; Godbillon, J.; Duval, M.; Schoeller, J.P.; Hirtz, J.; Bernier, J.J. Investigation of drug absorption from the gastrointestinal tract of man. I. Metoprolol in the stomach, duodenum and jejunum. *Br. J. clin. Pharm.* **1985**, 19, 97S-105S.

14. Farre, M.L.; Perez, S.; Kantiani, L.; Barcelo, D. Fate and toxicity of emerging pollutants, their metabolites and transformation products in the aquatic environment. *Trends Anal. Chem.* **2008**, 27, 991-1008.

15. Simazaki, D.; Kubota, R.; Suzuki, T.; Akiba, M.; Nishimura, T.; Kunikane, S. Occurrence of selected pharmaceuticals at drinking water purification plants in Japan and implications for human health. *Water Res.* **2015**, 76, 187-200.

16. Dehdashti, B.; Amin, M.M.; Pourzamani, H.R.; Rafati, L.; Mokhtari, M. Removal of atenolol from aqueous solutions by multiwalled carbon nanotubes modified with ozone: kinetic and equilibrium study. *Water Sci. Technol*. **2018**, 2017, 636-649.

17. Mouele, E.S.M.; Tijani, J.O.; Badmus, K.O.; Pereao, O.; Babajide, O.; Zhang, C.; Shao, T.; Sosnin, E.; Tarasenko, V.; Fatoba, O.O.; Laatikainen, K.; Petrik, L.F. Removal of pharmaceutical residues from water and wastewater using dielectric barrier discharge methods-a review. *Int. J. Environ. Res. Public Health* **2021**, 18, 1683.

18. Sotelo, J.L.; Ovejero, G.; Rodríguez, A.; Alvarez, S.; García, J. Removal of atenolol and isoproturon in aqueous solutions by adsorption in a fixed-bed column. *Ind. Eng. Chem. Res.* **2012**, 51, 5045-5055.

19. Norcom, G.D.; Dodd, R.I. Activated carbon for the removal of taste and odor. *Am. Water Works Assoc.* **1930**, 22, 1414-1437.

20. Homem, V.; Santo, L. Degradation and removal methods of antibiotics from aqueous matrices – A review. *J. Environ. Manage.* **2011***, 92, 2304-2347.

21. Plüss-Suard, C.; Pannatierb, A.; Kronenberg, A.; Mühlemann, K.; Zanetti, G. Hospital antibiotic consumption in Switzerland: comparison of a multicultural country with Europe. *J. Hosp. Infect.* **2011**, 79(2), 166-171.

22. Rajagopal, S.; Kuriacose, J.C. Catalysis by transition metal complexes: achievements and promises. *Curr. Sci.* **1981**, 50, 1047-1052.

23. Malinowski, J.; Zych, D.; Jacewicz, D.; Gawdzik, B.; Drzezdzon, J. Application of coordination compounds with transition metal ions in the chemical industry-a review. *Int. J. Mol. Sci.* **2020**, 21, 5443.

24. Andrade, M.A., Mestre, A.S.; Carvalho, A.P.; Pombeiro, A.J.L.; Martin, L.M.D.R.S. The role of nanoporous carbon materials in catalytic cyclohexane oxidation. *Catal. Today* **2020**, 357, 46-55.

25. Kalck, P.; Urrutigoïty, M. Tandem hydroaminomethylation reaction to synthesize amines from alkenes. *Chem. Rev.* **2018**, 118, 3833-3861.

26. Nasrallah, H.; Hierso, J.C. Porous materials based on 3-dimensional td-directing functionalized adamantane scaffolds and applied as recyclable catalysts. *Chem. Mater.* **2019**, 31, 619-642.

27. Dergunov, S.A.; Khabiyev, A.T.; Shmakov, S.N.; Kim, M.D.; Ehterami, N.; Weiss, M.C.; Birman, V.B.; Pinkhassik, E. Encapsulation of homogeneous catalysts in porous polymer nanocapsules produces fast-acting selective nanoreactors. *ACS Nano* **2016**, 10, 11397-11406.

28. Cai, G.; Ding, M.; Wu, O.; Jiang, H.L. Encapsulating soluble active species into hollow crystalline porous capsules beyond integration of homogeneous and heterogeneous catalysis. *Natl. Sci. Rev.* **2020**, 7, 37-45.

29. Derbe, T.; Temesgen, S.; Bitew, M. A short review on synthesis, characterization, and applications of zeolites. *Adv. Mater. Sci. Eng.* **2021**, 6637898.

30. Golbad, S.; Khoshnoud, P.; Keleney, G.; Abu-Aahra, N. Synthesis and characterization of highly crystalline Na-X zeolite from class F fly ash. *Water Environ. J.* **2020**, 34, 342-349.

31. Chen, L.; Xu, Q. Metal-organic framework composites for catalysis. *Matter.* **2018**, 1, 57-89.

32. Maurya, M.R.; Singh, B.; Adão, P.; Avecilla, F.; Costa Pessoa, J. Zeolite encapsulated copper(II) complexes of pyridoxal based tetradentate ligands for the oxidation of styrene, cyclohexene and methyl phenyl sulfide. *Eur. J. Inorg. Chem.* **2007**, 5720-5734.

33. Maurya, M.R.; Chandrakar, A.K.; Chand, S. Oxovanadium(IV) and copper(II) complexes of 1, 2-diaminocyclohexane based ligand encapsulated in zeolite-Y for the catalytic oxidation of styrene, cyclohexene and cyclohexane. *J. Mol. Catal. A: Chem.* **2007**, 270, 225-235.

34. Maurya, M.R.; Chandrakar, A.K.; Chand, S. Oxidation of methyl phenyl sulfide, diphenyl sulfide and styrene by oxovanadium(IV) and copper(II) complexes of NS donor ligand encapsulated in zeolite-Y. *J. Mol. Catal. A: Chem.* **2007**, 278, 12-21.

35. Maurya, M.R.; A. K. Chandrakar, Chand, S. Zeolite-Y encapsulated metal complexes of oxovanadium(VI), copper (II) and nickel (II) as catalyst for the oxidation of styrene, cyclohexane and methyl phenyl sulfide. *J. Mol. Catal. A: Chem.* **2007**, 274, 192-201.

36. Kosinov, N.; Liu, C.; Hensen, E.J.M.; Pidko, E.A. Engineering of transition metal catalysts confined in zeolites. *Chem. Mater.* **2018**, 30, 3177-3198.

37. Balkus, K.J.; Alexei, G.G. Zeolite encapsulated metal complexes. *J. Incl. Phenom. Macrocycl. Chem.* **1995**, 21, 159-184.

38. Li, C. Chiral synthesis on catalysts immobilized in microporous and mesoporous materials. *Catal. Rev. Sci. Eng.* **2004**, 46, 419-492.

39. Hassani, F.; Sharif, M.A.; Tabatabaee, M.; Mahmoodi, M. Encapsulation of a Cu(II) complex with 2,6-pyridine dicarboxylic acid in zeolite-X nanoporosity as an efficient heterogeneous catalyst for oxidation of aniline. *Iran. J. Catal.* **2021**, 1, 287-294.

40. Balkus, K.J.; Ly, K.T. The preparation and characterization of an X-type zeolite: An experiment in solid-state chemistry. *J. Chem. Edu.* **1991**, 68, 875-877.

41. Modi, C.K.; Trivedi, P.M. Synthesis, characterization and catalytic behaviour of entrapped transition metal complexes into the zeolite-Y. *Adv. Mater. Lett.* **2012**, 3, 149-153.

42. Aghabozorg, H.; Manteghi, F.; Sheshmani, S. A Brief Review on Structural Concepts of Novel Supramolecular Proton Transfer Compounds and Their Metal Complexes. *J. Iran. Chem. Soc.* **2008**, 5, 184-227.

43. Davidova, M.; Nachtigallova, D.; Bulanek, R.; Nachtigall, P. Characterization of the cu$^+$ sites in high-silica zeolites interacting with the co molecule: Combined computational and experimental study. *J. Phys. Chem.* B **2003**, 107, 2327-2332.

44. Ferreira, R.; Silva, M.; Freire, C.; de Castro, B.; Figueiredo, J.L. Encapsulation of copper(II) complexes with pentadentate N_3O_2 Schiff base ligands derived from acetylacetone in NaX zeolit. *Microporous Mesoporous Mater.* **2000**, 38, 391-401.

45. Huang, Y.; Jiang, Z.; Schwieger, W. Vibrational spectroscopic studies of layered silicates. *Chem. Mater.* **1999**, 11, 1210-1217.

46. Maurya, M.R.; Chandrakar, A.K.; Chand, S. Oxidation of phenol, styrene and methyl phenyl sulfide with H_2O_2 catalysed by dioxovanadium(V) and copper(II) complexes of 2-amino-methylbenzimidazole-based ligand encapsulated in zeolite-Y. *J. Mol. Catal. A Chem.* **2007**, 263, 227-237.

47. Chavan, S.A.; Srinivas, D.; Ratnasamy, P. A novel, zeolite-encapsulated μ3-oxo Co/Mn cluster catalyst for oxidation of *para*-xylene to terephthalic acid. *Chem. Commun.* **2001**, 12, 1124-1125.

48. Abbo, H.S.; Titinchi, S.J. Metallo Salicylidenetriazol Complexes encapsulated in zeolite-y: synthesis, physicochemical properties and catalytic studies. *Top. Catal.* **2010**, 53, 1401-1410.

49. Dittmeyer, R.; Grunwaldt, J.D.; Pashkova, A. A review of catalyst performance and novel reaction engineering concepts in direct synthesis of hydrogen peroxide. *Catal. Today* **2015**, 284, 149-159.

50. Miceli, M.; Frontera, P.; Macario, A.; Malara, A. Recovery/reuse of heterogeneous supported spent catalysts. *Catalysts* **2021**, 11, 591.